forecasting

MDPI

Article

Impact of PV and EV Forecasting in the Operation of a Microgrid

Giampaolo Manzolini *, Andrea Fusco, Domenico Gioffrè, Silvana Matrone, Riccardo Ramaschi, Marios Saleptsis, Riccardo Simonetti, Filip Sobic, Michael James Wood, Emanuele Ogliari and Sonia Leva

Department of Energy, Politecnico di Milano, 20156 Milan, Italy; andrea.fusco@polimi.it (A.F.); domenico.gioffre@polimi.it (D.G.); silvana.matrone@polimi.it (S.M.); riccardo.ramaschi@polimi.it (R.R.); marios.saleptsis@polimi.it (M.S.); riccardo.simonetti@polimi.it (R.S.); filip.sobic@polimi.it (F.S.); michael.wood@polimi.it (M.J.W.); emanuelegiovanni.ogliari@polimi.it (E.O.); sonia.leva@polimi.it (S.L.)
* Correspondence: giampaolo.manzolini@polimi.it

Abstract: The electrification of the transport sector together with large renewable energy deployment requires powerful tools to efficiently use energy assets and infrastructure. In this framework, the forecast of electric vehicle demand and solar photovoltaic (PV) generation plays a fundamental role. This paper studies the impact of forecast accuracy on total electric cost of a simulated electric vehicles (EVs) charging station coupled with true solar PV and stationary battery energy storage. The optimal energy management system is based on the rolling horizon approach implemented in with a mixed integer linear program which takes as input the EV load forecast using long short-term memory (LSTM) neural network and persistence approaches and PV production forecast using a physical hybrid artificial neural network. The energy management system is firstly deployed and validated on an existing multi-good microgrid by achieving a discrepancy of state variables below 10% with respect to offline simulations. Then, eight weeks of simulations from each of the four seasons show that the accuracy of the forecast can increase operational costs by 10% equally distributed between the PV and EV forecasts. Finally, the accuracy of the combined PV and EV forecast matters more than single accuracies: LSTM outperforms persistence to predict the EV load (−30% root mean squared error), though when combined with PV forecast it has higher error (+15%) with corresponding higher operational costs (up to 5%).

Keywords: optimal energy management system; LSTM; EV forecast; microgrid operation; PV forecast; MILP

Citation: Manzolini, G.; Fusco, A.; Gioffrè, D.; Matrone, S.; Ramaschi, R.; Saleptsis, M.; Simonetti, R.; Sobic, F.; Wood, M.J.; Ogliari, E.; et al. Impact of PV and EV Forecasting in the Operation of a Microgrid. *Forecasting* **2024**, *6*, 591–615. https://doi.org/10.3390/forecast6030032

Academic Editor: José-Santos López-Gutiérrez

Received: 14 June 2024
Revised: 12 July 2024
Accepted: 28 July 2024
Published: 31 July 2024

1. Introduction

The transportation sector is a major polluter, as it accounted for 28.51% of the total greenhouse gas emissions in 2021 in Europe [1]. The evolution of current transportation fleets to electric vehicles (EVs) (10% of the road vehicle fleet is expected by 2030 [2]) will accelerate the green transition and decarbonization of Europe. This rapid increase in EV adoption will considerably affect electric grids since a large charging network is required, with a special focus on optimal planning and operation of public charging stations (CSs). Therefore, it is essential to monitor and regulate the charging process, to exploit renewable energy sources (RESs) locally, and, where needed, to include stationary storage. Implementing novel emerging technologies for the optimization of the charging process is crucial for exploiting RESs, especially solar photovoltaic (PV) production [3], and stabilizing the grid [4]. EVs charging stations powered by the grid, PV, and a battery energy storage system (BESS) are analyzed by the scientific community from the placement [5], sizing [6], implementation [7], and energy scheduling [8] points of view, among others. From this perspective, CS integration is being investigated under the lens of microgrids (MGs) [9]. In the scientific literature on MGs, several works stressed the importance of optimizing MG operation [10], as well as the relevance of using accurate forecasting methods in the optimization of MG energy management [11,12]. Forecasting and optimization techniques

are also being developed considering the achievements in managing uncertainties in MGs [13].

Load forecasting plays a significant role in demand-side management (DSM) [14–16], where it serves as a crucial element in balancing load demand and power production.

EV load forecasting methods are categorized into traditional statistical models and artificial intelligence models [17]. Traditional models include time series analysis, autoregressive integrated moving average (ARIMA), regression analysis, Kalman filtering, and statistical methods, while artificial intelligence methods encompass artificial neural network (ANN), support vector machine, and deep learning (DL) models. Initially, statistical models were preferred due to limited EV charging data, necessitating the creation of realistic scenarios through computational algorithms [18]. However, with the greater availability of electric vehicle supply equipment (EVSE) load data, the focus has shifted to data-driven approaches, particularly ANNs, in EV power load forecasting research [19,20]. In [21], a review of EV scheduling, clustering, and forecasting, the authors report that artificial intelligence models have been the preferred approach for many researchers, as they perform better than other probabilistic models.

Long short-term memory (LSTM) recurrent neural networks (RNNs) appear to be exceptionally proficient in predicting load across diverse time series problems [22]. In [23], an LSTM model combined with feature engineering empirical mode decomposition (EMD) is benchmarked against seasonal autoregressive integrated moving average (SARIMA) obtaining a skill score up to 73% relative to 7-day persistence. The literature consistently demonstrates the superior performance of LSTM networks in the field of EVs charging forecasts. Hence, based on these findings, we have selected the LSTM model as the cornerstone of our work due to its demonstrated effectiveness and suitability for the task at hand.

Moving to the EVs charging optimization, the operation of CSs relying on PV and BESS was performed with several different methods and goals. Selected approaches generally aim to achieve cost minimization [24] or profit maximization [25] according to the use case, but also enhanced grid support through self-consumption [26] and charging scheduling [27] the effectiveness of pre-calculated schedules can be compromised by uncertainties in the arrival and departure times of EVs and fluctuations in energy demand. Therefore, real-time operation algorithms must have robustness with respect to load as well as forecast uncertainties, as described in the previous subsection.

Regarding optimization methods, probabilistic approaches are robust and reliable in uncertain environments but suffer from heavy computational time [28]. This drawback is partially solved by robust optimization (RO) [29]. Model predictive control (MPC) is extensively used for robustness and reliability obtained through the receding horizon approach but also suffers from high computational time. Therefore, MPC is often used as the later stage in a multi-stage formulation to amend the decision made by an earlier algorithm in real time. Other relevant methods are metaheuristics algorithms and fuzzy logic optimization [30,31].

Deterministic models, and mixed-integer linear programming (MILP) in particular, are still the most widely adopted because they can identify the global optimal solution given convexity and a continuously differentiable cost function, with computational time compatible with industrial applications. MILP models are used both in real-time operation [32] or in day-ahead scheduling as a first stage that can then be adapted in real time through an operation layer [33]. Indeed, a multiple-stage optimization considers the uncertain behavior of the PV production and EV demand providing an improved solution for real-time energy management.

While stochastic and robust optimization approaches offer a more accurate and modelically correct way to handle uncertainties, their computational complexity often makes them impractical for real-time optimization. These approaches require solving extensive scenario-based models or worst-case formulations, leading to significantly longer solution times. Therefore, despite their robustness, they are not feasible for applications needing

immediate decision-making. MILP, on the other hand, strikes a balance between accuracy and computational efficiency, making it suitable for real-time applications where timely decisions are crucial.

In this context, the predict-then-optimize (PTO) framework is still the most widely adopted to optimize this kind of systems. The PTO integrates prediction and optimization processes to enhance decision-making under uncertainty. In this framework, the prediction phase involves using statistical or machine learning models to forecast future uncertain parameters, such as demand, prices, or weather conditions. These forecasts are then input into an optimization model, which aims to find the best decision that minimizes cost or maximizes profit, given the predicted values. The key interaction between these two processes lies in how the predictions inform the optimization model. Accurate predictions lead to more effective optimization, as the optimization process relies on these forecasts to construct a solution that is robust against the predicted uncertainties. This interplay ensures that the optimization model is adaptive and responsive to future scenarios, thus enhancing the overall performance of the decision-making process.

Despite works on energy management system (EMS) validation and testing conducted in several universities and research centers (Public University of Navarre [34], Aalborg University [35], Center for Renewable Energy Sources and Saving (Athens) [36,37], and in Catalonia Institute for Energy Research [38]), there is still a lack of literature on the impact of prediction errors on microgrid operations, both in simulations and experimental facilities.

The scope of this work is to evaluate the impact of EV forecasting in the optimization framework, meaning that in addition to forecast skill these methods affect the operation of the microgrid from a technical and economic point of view. This paper evaluates how different EV forecast methods affect a sequential decision-making process, which is the outcome of a two-stage optimization tool. This study is performed on a physical MG located in Politecnico di Milano, Department of Energy [39], in addition to offline computer simulations.

This work is a novel contribution because the literature has yet to adequately cover how forecasting errors affect operational costs in a true functioning microgrid. While the predict-then-optimize approach is widely recognized, only a few studies have thoroughly examined its practical limitations. Notably, it is not well understood how the accuracy of load and solar forecasts influences the operational costs for a dynamic pricing electric tariff downstream of the optimizer and control equipment. Only a few papers have explored the error impact of different electric vehicle (EV) forecasting techniques within a hierarchical predictive control strategy aimed at optimizing microgrid operations. Finally, a significant distinction of this study compared to others is its real-time experimental validation and long-term simulation using highly accurate data from MG^{2}Lab. For instance, a significant gap in the literature is the use of true building-scale microgrids in testing. In [40], a microgrid EMS is designed and implemented in a small bench-top testbed and further implanted at a commercial building with a maximum 300 kW load; however, all of the DERs are hardware-in-the-loop simulated by power converters rather than by true batteries and solar PV modules. The results are therefore much more credible than just a software simulation but lack some of the characteristics and uncertainty when controlling true Li-ion electrochemical cells and true silicon PV cells. Attempting to cover these gaps, the paper presents a comprehensive analysis of EV forecasting techniques error impacts, a comparative analysis and experimental validation between two methodologies (LSTM and persistence), and a long numerical analysis based on historical data.

The remainder of the article is structured as follows. Section 2 presents the optimization and forecasting methodologies employed in the energy management system of the proposed case study, described in Section 3. In Section 4, the model implementation is explained, as well as how the experimental testing facility is used. Section 5 includes the relevant results of this work, which is summarized and concluded in Section 6.

2. Methodology

2.1. Optimal Dispatch

The microgrid employs a two-layer EMS, previously described in [41], based on a rolling horizon (RH) approach where the first layer of the EMS is run every 15 min. The first layer determines the optimal dispatch of the BESS over the next 24 h, taking as input the forecast of both the EV load and PV generation, to minimize the operational cost of the system. The optimizer always takes into account technical constraints. However, as power unbalances inevitably arise due to forecast errors it is necessary to adopt a second layer to correct these unbalances in real time.

The first layer adopts an MILP formulation where variables model different power flows within the system (e.g., PV production, import/export from/to the grid, charge/discharge of the BESS). The optimal operation of the microgrid over the optimization horizon is evaluated by minimizing the total operational costs:

$$OF = min\left(\sum_{t \in \mathcal{T}_1} \Phi_t^{Opex}\right) \tag{1}$$

where:

$$\begin{aligned}\Phi_t^{Opex} &= c_t^{purch} \cdot P_t^{grid,purch} \cdot dt_1 - r_t^{sell} \cdot P_t^{grid,sell} \cdot dt_1 \\ &+ \sum_{es \in \mathcal{ES}} \left[c_{es}^{TP} \cdot P_{es,\,t}^{disch} \cdot dt_1 + \rho^{dev} \cdot SOE_t^{dev}\right] \\ &+ c^{curt} \cdot ND_{nd,t}^{curt} \cdot dt_1 + c^{UD} \cdot UD_t \cdot dt_1\end{aligned} \tag{2}$$

The main components of the aforementioned and following equations are explicitly stated in the Appendix A.

Meanwhile, the total operational cost Φ_t^{Opex} associated to each timestep t is given by the sum of four main components:

- $c_t^{purch} \cdot P_t^{grid,purch} \cdot dt_1 - r_t^{sell} \cdot P_t^{grid,sell} \cdot dt_1$ represents the cost and revenue (negative cost) coming from the withdrawal and injection of power from/into the grid;
- $\sum_{es \in \mathcal{ES}} \left[c_{es}^{TP} \cdot P_{es,\,t}^{disch} \cdot dt_1 + \rho^{dev} \cdot SOE_t^{dev}\right]$ is the sum of the BESSs' throughput-based O&M cost, and penalty cost associated with their state of energy (SOE) deviations;

$c^{curt} \cdot ND_{nd,t}^{curt} \cdot dt_1 + c^{UD} \cdot UD_t \cdot dt_1$ are penalty costs for curtailment of RES generation and unmet demand.

Forecasted PV production is an input to the EMS and can be curtailed if necessary. The BESSs are modeled on an energy basis with self-discharge efficiency, and separate charge/discharge efficiencies which are a function of battery power, that are evaluated through piecewise linear interpolation. To avoid damage, constraints are imposed to limit the state of charge (SOC) between lower and upper bounds and the maximum power that can be charged/discharged by the BESS. In addition, there is a constraint to ensure a balanced SOC between the two BESSs. Interaction with the electrical grid is constrained by setting a maximum value on the power that can be imported/exported by the microgrid. Details about the mathematical formulation of the constraints and detailed nomenclature can be found in Appendix A: Energy Management System.

The second layer is a heuristic approach taking as input BESS and grid setpoints determined by the first layer as well as discrepancies between the PV and EV load forecasts and the actual values. Depending on the signs and magnitude of these errors, the microgrid can be either in "power excess", where the inbound power flows are higher than the outbound ones, or in "power deficit". The logic adopted is to keep the first layer setpoint of power exchanged with the electrical grid. First, either the unmet demand or PV curtailment is reduced in the case of "power excess" and "power deficit", respectively. If that this is not enough, or if unmet demand and PV curtailment set by the first layer are equal to zero, the BESSs intervene to reduce the power balance. When the BESSs cannot correct the unbalances then the setpoint of the power exchanged with the grid is modified. Lastly, in

the extreme case of unbalance even after all the previous points, either PV curtailment or unmet demand is increased in the case of "power excess" and "power deficit", respectively.

2.2. EV Forecasting

2.2.1. LSTM with Attention

The EV charging power forecast is performed by an LSTM encoder–decoder with attention, inspired by Bahdanau [42]. The mathematical formulation of the LSTM and attention mechanism is described in Appendix B: EV Charging Forecaster. Each encoder and decoder is a single-layer LSTM of 24 hidden units, a value chosen by hyperparameter optimization. Training is performed with the Adam optimizer and early stopping to limit overfitting. The input vector is the most recent 3 days of EV charging power measurements and time-keeping variables such as day of week and time of day. The output vector is the next three days of charging power values. Power is always a 15 min interval average power time series. The training data subset is the EV charging load data in Section 4.2, less than 8 weeks—from each winter, spring, summer, and autumn—which are used for the test data subset. The model is trained using an early stopping criterion which monitors the validation loss, calculated on the final 20% of the training subset.

2.2.2. Persistence

The benchmark forecast model is naive persistence, which estimates any timestep t as equal to the past timestep $t - l$, where l is the lag value or the number of timesteps in the past. In a modified version sometimes called seasonal persistence, the lag value l is chosen to match an appropriate seasonality in the data, often daily or weekly for electric consumption. In the present case study, the EV charging data present a strong weekly seasonality; therefore, the value of lag is chosen equal to 672 steps (7 days). The timestep t is forecasted with the measurement from $t - 7d$ or $t - 168$ if the time series interval is 1 h. This is described in Equation (3), where $y_{forecast}$ is the forecasted value and y_{true} the measured one.

$$y_{forecast}(t) = y_{true}(t - l) \tag{3}$$

While it is possible to use persistence for a day-ahead solar PV forecast, the benchmark would not be very useful. Weather conditions in many climates, including the humid subtropical designation of the solar plant in this study, can change dramatically between consecutive days, so even very poorly trained solar PV forecast models could outperform 1-day persistence. Persistence is more common for solar nowcasting where the time horizon is 1 to 60 min.

2.3. PV Forecasting

The solar PV forecast is a hybrid physical–regression method developed and validated on the Multi-Good MicroGrid Laboratory (MG^2Lab) microgrid in [43]. The model outputs a day-ahead solar production time series at 15 min intervals. The model inputs are a numerical weather forecast for the location, physical plant specifications from the PV modules, and the most recent day of solar production time series. The model provides the solar production forecast based on numerical weather prediction for the week ahead at the considered locations and clear-sky radiation (CSR) of the plane of arrival to the array. The numerical weather forecast is from the European Center for Medium-Range Forecasts [44] and it is provided by a private company. The PV forecasting tool uses the global horizontal irradiance (GHI), air temperature, wind direction and speed, precipitation, humidity, and pressure. The list of the employed data is added in the following Table 1. A share of 80% of the whole dataset is used for the training and the remaining 20% for the validation.

Table 1. List of employed data.

Input	Parameters	Units of Measure
Deterministic	Global horizontal irradiance Clear-sky solar radiation	W/m^2
Weather forecasts	Relative humidity	%
	Wind direction	degree
	Pressure	Pa
	Rain	mm
	Wind speed	m/s
	Ambient temperature	Celsius
	Global horizontal irradiance Solar radiation	W/m^2

The CSR model is based on reference evaluation of solar transmittance, 2 bands (REST2) that considers more variables than similar atmospheric models and is validated by the literature as one of the best-performing CSR models [45]. Finally, the GHI must be tilted to the plant-of-arrival of the solar plant, given its azimuth and tilt angles.

The ANN is trained daily on the previous day's measured values in a supervised learning fashion, such that the weights and biases are optimized to produce a series of past outputs given past inputs. The ANN is retrained once per day to learn short-term patterns, such as a weather forecast which is consistently under estimating temperature.

2.4. Predict-Then-Optimize Approach

In this work, the predict-then-optimize framework, which integrates forecasting models and optimization techniques, has been adopted to enhance decision-making under uncertainty while maintaining computational tractability for implementation in an experimental facility. In this context, forecasts of EV load and PV generation, as described in Sections 2.2 and 2.3, are used as inputs for the optimization process.

In particular, the EMS employs a rolling horizon (RH) approach where the first layer (where the optimization phase is performed) utilizes these forecasts within an MILP formulation to evaluate the optimal operation of the microgrid, including PV production, grid interactions, and BESS operations. The MILP model ensures that the first layer of the EMS can find a globally optimal solution under the given forecasted conditions, balancing the operational costs defined in Section 2.1. The real-time adjustments are then handled by the second layer, which corrects any discrepancies arising from forecast errors, thereby maintaining system balance and operational efficiency.

3. Error Metrics

Statistical error metrics are necessary for training forecasting models and provide a summary of forecast performance to compare to other works in the literature. In the equations below, y is always a time series of true measurements or forecasted values and n is the length of the series.

- Root mean squared error (*RMSE*) is the square root of the mean squared error (MSE), making the units of RMSE the same as the data for a helpful comparison. Since it is closely related to the MSE which is used to train the LSTM, RMSE will also closely reflect how well a model was trained;

$$RMSE = \sqrt{\frac{1}{n}\sum\left(y_{true} - y_{forecast}\right)^2} \quad (4)$$

- Mean absolute error (*MAE*) is also reported here because it is common in the literature and very intuitive, giving equal weight to large and small errors;

$$MAE = \frac{1}{n}\sum\left|y_{true} - y_{forecast}\right| \tag{5}$$

- Symmetric mean absolute percentage error (*SMAPE*) is somewhat contested in the literature and there is no one single definition. However, the following definition is adequate because in this application there is no practical or theoretical problem with negative SMAPE values. Since all SMAPE definitions have terms in the denominator it is necessary to omit from the metric timesteps when the sum of y_{true} and $y_{estimated}$ is zero.

$$SMAPE = \frac{100}{n}\sum\frac{\left|y_{true} - y_{forecast}\right|}{0.5\left(y_{true} + y_{forecast}\right)} \tag{6}$$

4. Experimental Setup and Case Study

This section presents the case study investigated in this work as well as the testing facility, located at Politecnico di Milano (Milan, Italy), where the experimental activities have been carried out. The MG^{2}Lab setup available in the Department of Energy of Politecnico di Milano integrates different distributed energy resources like solar PV, combined heat and power, BESS, and hydrogen storage. Details about the microgrid, which can be operated both grid-connected or grid-islanded, can be found in [43].

4.1. Experimental Facility and Model Implementation

The selected MG^{2}Lab's components, as well as the structure of the EMS used for managing operation of the components, are presented in Figure 1.

Specifically, the setup comprises the following units:

- Grid connection: limited to 100 kW, used for withdrawing or injecting power from/to the distribution grid;
- Non-dispatchable RES: two PV arrays, both installed on the building roofs of 23 and 25 kW_p;
- Storage: two lithium-ion BESSs (BESS1 and BESS2) of 70 and 67.5 kWh, with a C-rate (C-rate is the rate of time in which the BESS takes to charge or discharge) equal to one and a minimum and maximum SOC equal to 35% and 85%, respectively. This results in an overall storage capacity of 68.75 kWh;
- Load: simulated using a back-to-back (B2B) converter, which is a programmable load following the setpoints of an EV load dataset, scaled to a 25 kW maximum power.

The EMS consists of three different modules, namely the load forecaster, PV forecaster, and optimizer. These are implemented in Python and deployed on the microgrid PC, which communicate with each other through a MySQL database used for storing/handling data. The load forecaster module contains two different forecasting models, LSTM and persistence. The LSTM is implemented in TensorFlow, which is an open-source library by Google used to build and deploy machine learning models [46]. The LSTM and persistence models run every hour providing a load forecast for the following 1.5 days. The solar forecasting module utilizes the physical hybrid artificial neural network (PHANN) model described in [47] and implemented using TensorFlow. It runs twice a day following weather forecast updates and provides the PV forecast for the following seven days. The optimizer module is divided into the first and second layers, where the first layer is implemented in the Python-based open-source optimization library Pyomo [48]. It runs every 15 min considering an optimization horizon of 24 h. On the other hand, the second layer is used for real-time power balancing and therefore it is implemented using a programmable logic controller (PLC) with a frequency of 100 milliseconds. It communicates with the MySQL database to obtain the setpoints provided by the first layer and both the forecasted and

measured values of the load and PV to perform the power balancing function. Additionally, a human–machine interface (HMI) is used to monitor the status of the microgrid and provide real-time measurements for the preliminary analysis of the results.

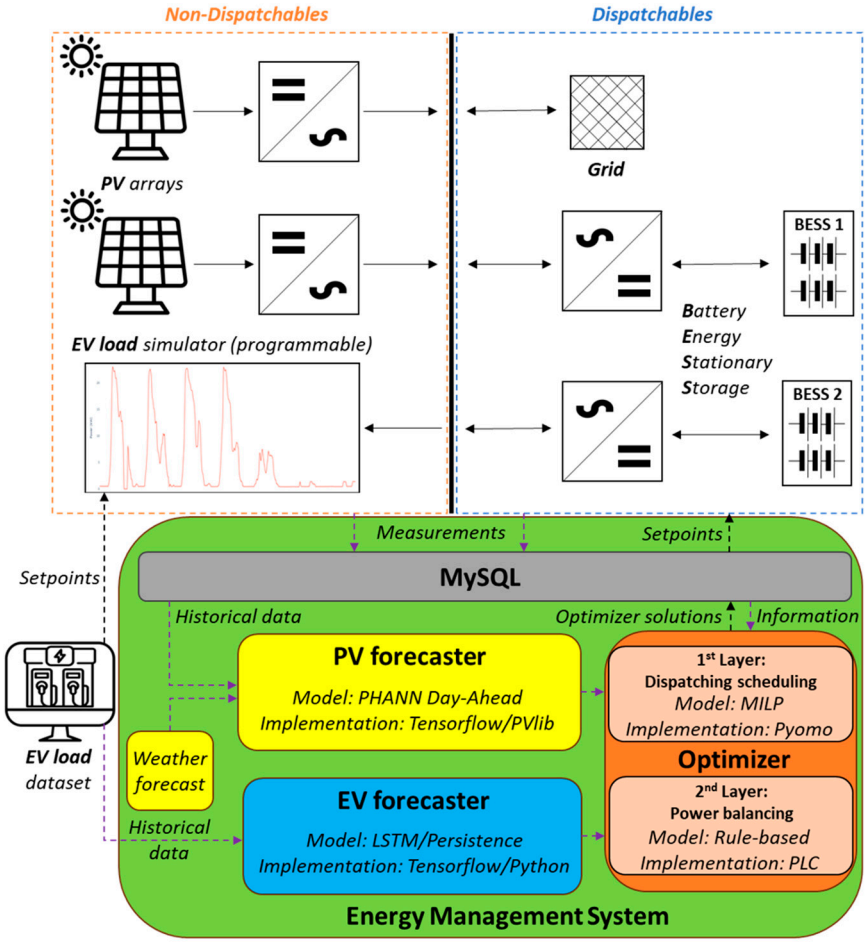

Figure 1. Experimental setup and control architecture considered in this case.

4.2. Case Study Description

The case study represents an EV charging station powered by the grid, PV, and BESS. The EV load is based on the records from the JPL (Jet Propulsion Laboratory) database from the adaptive charging network (ACN) [49]. This site has 52 EVSEs and is only accessible by employees, making it a good representation of a typical workplace schedule. The power curve of all 52 EVSEs is aggregated to reconstruct the whole charging station demand. However, only a subset of all the available data is considered suitable for the case study due to the anomalies associated with the COVID-19 pandemic. The considered set includes the sessions from 3 December 2018 to 4 January 2020. To accommodate the charging station demand within the MG^{2}Lab capabilities, the aggregated load power is scaled to a maximum of 25 kW.

The cost of purchasing the electricity from the grid is assumed to be twice the Italian national unified price (Prezzo Unico Nazionale, PUN) to account for transmission and other costs, while the revenue from selling electricity to the national grid is set equal to the zonal price (Prezzo Zonale, PZ) of the North region. These costs are taken from the Italian electricity market [50] for the year 2023.

In Table 2, values and profiles of the typical weekly EV load and prices are provided.

Table 2. Main features of the EV load and electricity prices of the considered cases in the study.

EV load	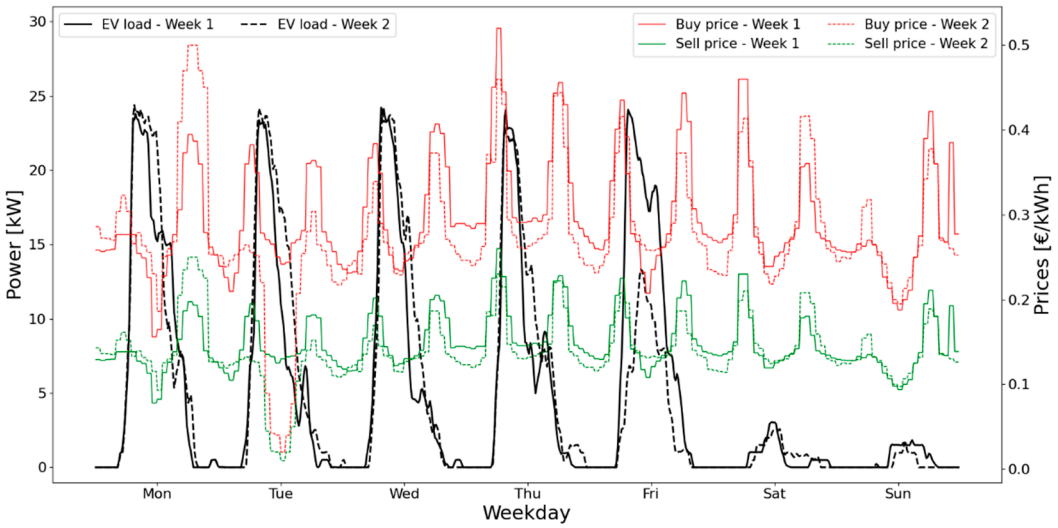	
	Typical week trends from the JPL dataset (scaled to 25 kW according to MG^{2}Lab size). Energy consumption for week 1 amounts to 842.5 kWh, while for week 2 it amounts to 823 kWh. Given EV charging at a workplace, there is a substantial difference between workdays (Monday–Friday) and weekend days (Saturday and Sunday). Weekend days are also very unpredictable. Fridays are also unpredictable in terms of magnitude, while the shape remains similar.	
Prices	Buy	Maximum: 0.666 €/kWh, minimum: 0.005 €/kWh, average: 0.255 €/kWh
	Sell	Maximum: 0.333 €/kWh, minimum: 0.003 €/kWh, average: 0.128 €/kWh

Both online and offline simulations are carried out to support the methods developed in this work. Online simulations means that the EMS and forecasting are implemented in the MG^{2}Lab experimental facility under real conditions, while offline simulations are computer-based using real data as input.

Online simulations aim to demonstrate that the developed models, including the different PV and EV forecasting methods, can be deployed in real system operation. The online simulations were run for two weeks on the MG^{2}Lab microgrid with either the persistence or LSTM models to predict the EV load. In both weeks, the same EV load was programmed for consistency. On the contrary, the PV production and forecast were from the true irradiance at the MG^{2}Lab. Measurements from the online experiment are then used for running offline simulations with both forecasters for comparison and validation of the approach. A summary of the considered weeks is reported in Table 3.

Table 3. Characteristics of the simulations performed in this work.

Simulation	**Offline**				**Online (MG^{2}Lab)**	
Goal	Assess the impact of each forecast method in the overall optimization Impact of combining PV and EV forecasting				Validate the method and demonstrate the application of the EMS with PV and EV forecasting	
Weeks	Winter	Spring	Summer	Autumn	24 February 2024– 1 March 2024	5 March 2024– 11 March 2024
PV data	Two-week MG^{2}Lab historical data for each season				MG^{2}Lab PV plant	
EV data	Two-week data for each season from the JPL dataset				JPL dataset: 10 December 2018–16 December 2018	
PV forecaster	PHANN day-ahead (MG^{2}Lab) and HML				PHANN Day-Ahead	
EV forecaster	Persistence and LSTM and HML				Persistence	LSTM

Offline simulations indicate the influence of EV load forecasts in different conditions by comparing the different forecasters over eight weeks, two from each season of the year. Simulations are carried out integrating the PV and EV load forecasts resulting from the JPL EV dataset and the measurements at MG^{2}Lab's PV field consistent with the season (i.e., for winter, two weeks of actual PV production in winter 2023 from the MG^{2}Lab's PV field and two winter weeks from the JPL database for EV load simulation are taken). The offline simulator, for each season, also considers different EV forecasting methods (see Table 2): persistence and LSTM forecast methods are considered. In addition, to have a benchmark case, a perfect forecast for both PV and EV is introduced, referred to as hourly mean lookahead (HML), where the perfect forecast predicts the exact average of PV and load measurements over 15 min. As the error metrics are based on forecasted data (averaged over 15 min) and measured data (discretized in 1 min intervals), statistical error metrics can never be zero even for the HML forecast, unless all measurements within the same 15 min interval are exactly equal to their average value. The case with the HML forecast for both PV and EV represents a lower bound for the simulations.

In this way, the offline simulations, besides showing the accuracy of each separate forecaster, show the combined statistical accuracy of PV and EV forecasting methods, the EV station operational costs, and quantify the impact of the forecast accuracy with respect to the ideal case.

Since the EMS adopts a rolling horizon approach, the residual SOC of the BESSs at the end of the simulation could not be imposed a priori; therefore, as different combinations of PV and load forecasts can lead to different final storage SOC, the difference between initial and final storage content is then accounted as an equivalent energy import from the grid, and it is valued at the minimum value of the import price over the entire simulation period.

For each case study, the following results have been reported:

- Statistical performances of PV;
- Load;
- Total net electrical forecast defined as

$$\varepsilon_{tot} = \left(\hat{PV}_{for} - PV_{meas}\right) - \left(\hat{Load}_{for} - Load_{meas}\right)$$

- Total operating costs;
- Operational schedule of the system.

5. Results

In this section, the numerical and experimental results of the comparison of the different EV load forecasts implemented in the deterministic EMS approaches are presented.

5.1. Online Simulations

Measurements of the experimental campaign with the LSTM forecast are reported in Figure 2 (the case with persistence is not reported for brevity). The results are shown to demonstrate that results between the EMS operating in the microgrid with all the physical components and the simulations are consistent. Therefore, simulation results performed offline can be considered representative of the real operation of a microgrid.

Some general considerations can be noted while comparing the experimental results with the corresponding offline simulations:

- On weekdays, when the electrical load is high, the microgrid imports electric energy at night when the electricity price is lower to charge the batteries, which are then discharged during the day in the absence of photovoltaic production;
- Minor differences between the two figures occur and are related to the parasitic losses of the battery power supply systems and other equipment in the laboratory where the microgrid operates (mainly during night-time). The battery charging process measured in the experimental campaign is spread over more hours compared to the

results of the simulation. Nevertheless, the quantities of electrical energy are nearly identical and the effect on the simulation results is negligible.

The overall energy and economic results for the different approaches tested in the microgrid are summarized in Table 4. Despite the identical load data used for each online week, there are small differences between simulations and experiments as the B2B converter requires a small amount of Gaussian noise added to the programmed load profile.

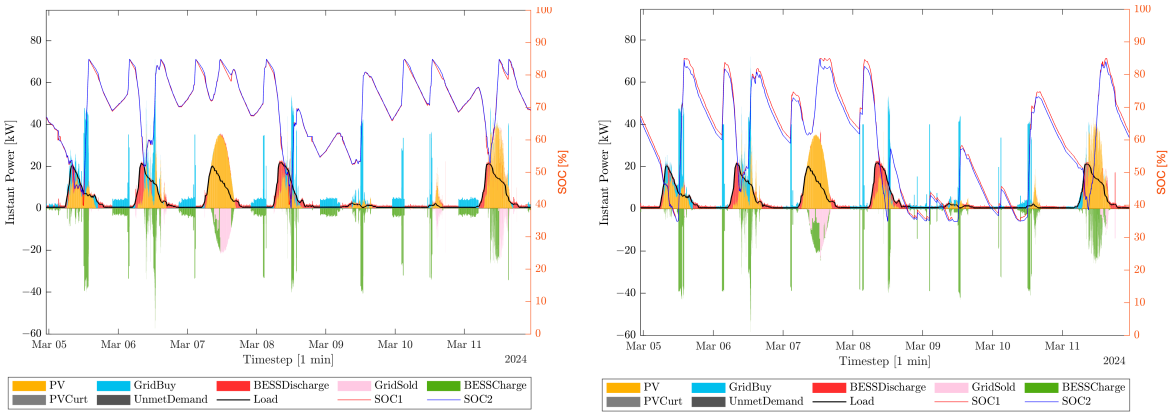

Figure 2. Operational scheduling for a considered week using LSTM forecast: experimental results (**left**) and offline results with the simulator (**right**).

Table 4. Overall results of the experiments and the corresponding simulations. Note that the persistence EV forecast is not identical among the two weeks because of small variations in the B2B converter output power.

	Week 1: 24/02/2024–01/03/2024		**Week 2: 05/03/2024–11/03/2024**	
	Persistence Experimental	**Persistence Simulated**	**LSTM Experimental**	**LSTM Simulated**
EV load [kWh]	709.04	709.03	709.34	709.33
PV production [kWh]	330.28	326.68	700.63	697.04
EV forecast SMAPE [%]	39.76	41.69	54.94	52.37
PV production SMAPE [%]	111.44	111.44	195.46	195.46
Electricity purchased [kWh]	900.78	818.07	561.41	505.33
Electricity sold [kWh]	106.74	65.77	142.02	83.01
Initial SOC [kWh/%]	18.0/51.3	18.0/51.3	23.4/66.9	23.4/66.95
Final SOC [kWh/%]	22.3/63.7	13.4/38.2	24.2/69.1	21.81/62.3
Unmet demand [kWh]	0.00	0.00	0.00	0.00
Curtailment [kWh]	0.01	0.00	0.01	0.00
Purchased electricity [€]	240.24	213.35	127.44	112.92
Sold electricity [€]	18.66	10.74	19.01	12.19
Unmet demand [€]	0.00	0.00	0.00	0.00
Curtailment [€]	0.06	0.00	0.05	0.00
BESS residual [€]	−2.17	2.28	−0.46	1.13
Total [€]	219.47	204.88	108.02	96.24

Finally, the operational costs of the offline simulations are in agreement with the experimental facility (i.e., Experimental), with differences below 10%. Considering that

several systems and controllers present in the microgrid cannot be reasonably simulated offline, these results validate the proposed approach which can then be extended to the yearly simulations.

5.2. Offline Simulations

Once the MG^{2}Lab approach was validated, offline simulations were conducted to assess the impact of the considered PV and EV forecasting methodologies by extending the analysis over a wider period. Results for two weeks in spring are presented, followed by the overall performance of the other three weeks.

Spring Case

For the spring season, the statistical performance indexes of the PV, load, and net load (combination of load and PV) forecasts are reported in Table 5.

Table 5. Statistical performance of PV and EV forecasters (single and combined). The PV and EV forecasts are evaluated independently in the first five rows. The remaining rows are the sum of the PV and EV forecasts, which is commonly referred to as the net load. Note that the HML forecast error is nonzero because of the discrepancy between the forecast time discretization (15 min) and the experimental data sampling (1 min).

	Forecast	MAE	SMAPE	RMSE
PV	PHANN	4.10	71.91	7.49
	HML	0.72	6.85	2.13
EV	Persistence	1.58	44.89	3.23
	LSTM	1.06	44.66	1.87
	HML	0.16	7.33	0.35
PV+EV	PV HML + EV persistence	1.94	−69.67	3.87
	PV HML + EV LSTM	1.44	−30.41	2.82
	PV HML + EV HML	0.76	0.29	2.15
	PV PHANN + EV persistence	2.88	−7.73	5.27
	PV PHANN + EV LSTM	4.30	−388.93	7.63
	PV PHANN + EV HML	2.37	35.51	4.60

As it is possible to notice, LSTM outperforms persistence in all the statistical performance parameters. However, when coupled with the PHANN day-ahead PV forecast, it results in a higher net electrical load forecast error among all the predictors. This first result suggests the importance of considering accuracy indexes accounting for the overall forecast and not focusing on each forecaster separately. Similarly, the calibration and development of the forecast tools shall account for the whole system and not only the specific good predicted.

Results of the offline simulations for a spring week (out of the two considered) are reported in Figure 3. The operational scheduling for both methods is quite similar across the different days of the week, except for some minor quantitative differences in the net electricity imported from the grid, which appears to be slightly lower in the persistence case.

However, the major difference can be seen on 7 April: in the operational scheduling with persistence, the EMS imports electricity from the grid only in the first hours of the day

to meet the load, then the BESSs are discharged in the following hours. The operational scheduling of the LSTM (right) is different, as the EMS imports electricity from the grid throughout the day without discharging the BESSs, resulting in higher operational costs, as summarized in Table 6.

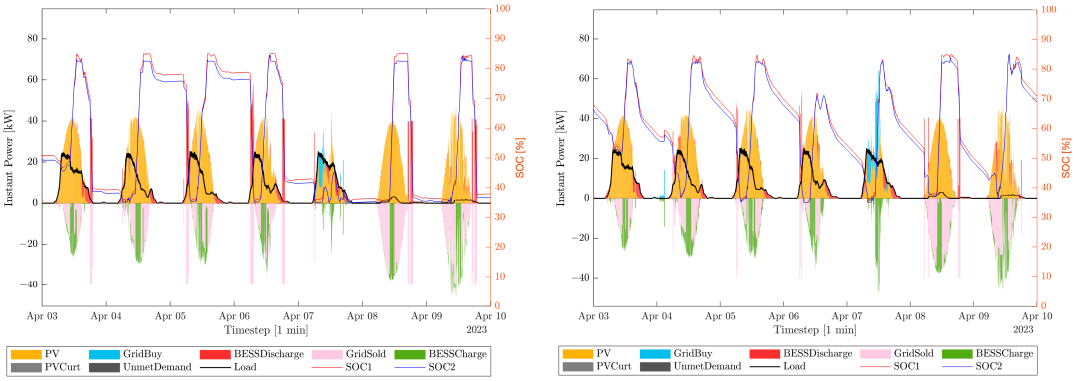

Figure 3. Offline results of the operational scheduling of the two weeks of spring using persistence (**left**) and LSTM (**right**) forecasts.

Table 6. Overall results of the experiments and the corresponding simulations.

PV Forecast		**HML**			**PHANN**	
Load Forecast	**Persistence**	**LSTM**	**HML**	**Persistence**	**LSTM**	**HML**
EV load [kWh]	1665.24	1665.24	1665.24	1665.24	1665.24	1665.24
PV production [kWh]	3328.39	3328.39	3328.39	3328.39	3327.34	3328.39
Electricity purchased [kWh]	214.59	214.88	144.99	184.22	176.48	150.00
Electricity sold [kWh]	1830.40	1833.37	1771.80	1774.63	1740.01	1757.46
Total BESSs losses [kWh]	57.22	53.86	46.44	75.56	86.79	65.65
Initial SOC [kWh/%]	17.5/50.0	17.5/50.0	17.5/50.0	17.5/50.0	17.5/50.0	17.5/50.0
Final SOC [kWh/%]	12.56/35.9	12.90/36.9	12.45/35.6	16.09/46.0	23.39/66.8	12.52/35.8
Unmet demand [kWh]	0.00	0.00	0.00	0.00	0.00	0.00
Curtailment [kWh]	0.00	1.05	0.00	0.00	1.05	0.00
Purchased electricity [€]	50.61	48.34	29.14	47.42	51.47	35.07
Sold electricity [€]	278.30	279.24	267.79	265.40	253.35	261.38
Unmet demand [€]	0.00	0.00	0.00	0.00	0.00	0.00
Curtailment [€]	0.00	0.00	0.00	0.00	0.00	0.00
BESS residual [€]	0.40	0.37	0.40	0.11	-0.47	0.40
Total [€]	−227.29	−230.54	−238.35	−217.87	−202.35	−225.91

As the PV forecasts used to perform these simulations were the same for both case studies, the higher import from the grid during the EMS–LSTM operations was only related to the accuracy of the net electrical load forecasts. This difference, which results in higher operational costs, can be attributed to two main factors:

1. Purchase and sale prices fluctuate throughout the 24 h cycle, with this dynamic being particularly pronounced during the spring season. In fact, as it is possible to see from the table above, the EMS with persistence imports electricity at an average price of 0.257 €/kWh and exports to the grid at 0.15 €/kWh, while the average price for the EMS with LSTM is 0.292 €/kWh with a similar value when exporting. This is because the overall LSTM errors may be lower in absolute value compared to those

of persistence, but they are more pronounced during the hours of the day when electricity prices are significantly higher (for purchases), therefore resulting in a more relevant impact;

2. The accuracy of the net load forecasts is not the algebraic result of PV and EV forecasts: errors can amplify or reduce depending on the particular case. For instance, in the persistence case, errors in PV and load forecasts may exhibit opposite signs, potentially mitigating the overall inaccuracies of the individual forecasters. In fact, when considering a perfect HML PV forecast, the EMS with LSTM demonstrates slightly lower operational costs.

Overall, the optimal case for the considered two spring weeks occurs for LSTM when coupled with the HML PV forecast, while persistence performs better when coupled with the PHANN PV forecast. This is another indication of the necessity to incorporate system management costs into the error function of forecasting algorithms, to reduce the errors associated with expensive balancing costs.

6. Overall Results

Below are the overall forecast accuracy and the economic operation results, respectively, for all the seasons, as summarized in Table 7.

Table 7. Accuracy of the adopted forecast tools for the combined net load of different seasons (top) and corresponding economic results (bottom). Note that the combined HML PV and HML EV forecast error is nonzero because of small differences between the input and output of the back-to-back converter.

Net Load Forecast Error (RMSE in [kW])						
PV forecast		HML			PHANN	
EV forecast	Persistence	LSTM	HML	Persistence	LSTM	HML
Spring	3.87	2.82	2.15	5.27	7.63	4.60
Summer	3.39	2.22	1.38	4.89	5.05	3.78
Autumn	3.64	2.25	1.25	5.16	5.71	3.80
Winter	2.87	4.40	0.93	4.68	4.48	4.23
Economic result (€)						
PV forecast		HML			PHANN	
EV forecast	Persistence	LSTM	HML	Persistence	LSTM	HML
Spring	−227.29	−230.54	−238.35	−217.87	−202.35	−225.91
Summer	−197.85	−199.21	−201.44	−187.02	−181.94	−191.97
Autumn	46.5	44.86	38.92	48.49	49.68	43.90
Winter	218.31	216.65	205.86	218.19	218.15	215.59

Looking at the tables, the following conclusions can be drawn:

- There is a good correspondence between the overall net electric errors and the economic results. The higher the accuracy of the combined forecast error the worse the operational cost; LSTM performs better when the HML PV forecast is assumed, while it is worse than persistent when the PHANN PV forecast is adopted;
- The impact of EV and PV forecasts is pretty similar on the economic results when compared to the ideal case: in both cases, the difference in operating costs between using perfect and actual forecasts is around 5%;
- The combination of PV and EV forecasts might lead to discrepancies up to 10% with respect to the ideal case.

Overall, these results suggest that the accuracy of a stand-alone forecast model is not relevant when it works in combination with other forecasters. Moreover, forecasters which

have higher accuracy are outperformed by others when the accuracy of the prediction is time-relevant as this is for energy systems with varying electricity prices. Therefore, it is important to correctly predict the load or PV production when electricity prices are high and this aspect should be accounted for when training the forecast methods.

7. Conclusions

Currently, the predict-then-optimize approach remains one of the most widely adopted techniques for operational optimization in multi-energy systems. Although some conceptual limitations of this approach have been noted in the literature, few papers have attempted to investigate the impact of both load and solar forecast accuracy on the operational cost of an existing microgrid.

In this study, a detailed analysis has been conducted of the error impact of various EV forecasting techniques within a hierarchical predictive control strategy to optimize an EVs charging station microgrid operation. The analysis presented herein comprised an experimental part, during which two methodologies under investigation (LSTM and persistence) were tested within the experimental facility of the MG^2Lab. Additionally, a simulation study was conducted extending the numerical analysis over a longer period, considering historical data collected in the laboratory in 2023.

The first relevant result of the study was the validated operation of a multi-good microgrid using both PHANN PV and LSTM EV load prediction combined with an EMS operated to minimize the operational costs. This confirmed that the methods developed are of interest for the quantitative results but can also be deployed in real systems.

Quantitative results showed that the accuracy of the combined forecast models matters: higher combined accuracy resulted in higher performance of the EMS with better operational results.

In addition, the accuracies of the different forecasters do not individually correlate with final performance. It was shown that LSTM has the highest accuracy in predicting the EV load; however, the EMS operating with the LSTM EV forecast can have the poorest performance when coupled with the PHANN PV forecast. Besides the interactions, LSTM is less accurate than persistence when electricity prices are high, resulting in higher operational costs.

Future works will focus on the development of new customized loss functions to train and evaluate forecasting models. These will depart from generic statistical performance metrics, aiming instead to capture downstream decision-maker dynamics, thereby providing forecasts that are optimized for the selected application. Initial investigations suggest this will result in a more integrated and cost-effective synergy between forecasting and optimization procedures.

Author Contributions: Conceptualization, G.M. and E.O.; methodology, G.M., E.O. and S.L.; software, A.F., D.G., S.M., R.S. and M.J.W.; validation, A.F., D.G., S.M., R.S. and M.J.W.; formal analysis, A.F., D.G., S.M., R.R. and M.J.W.; investigation, G.M.; writing—original draft preparation, G.M., A.F., D.G., S.M., M.S., F.S. and M.J.W.; writing—review and editing, E.O.; visualization, A.F., D.G., S.M., R.R. and M.J.W.; supervision, G.M. and E.O.; project administration, S.L.; funding acquisition, G.M. and S.L. All authors have read and agreed to the published version of the manuscript.

Funding: This research received no external funding.

Data Availability Statement: The raw data supporting the conclusions of this article will be made available by the authors on request.

Acknowledgments: This study was carried out within the MOST—Sustainable Mobility Center and received funding from the European Union Next-GenerationEU (PIANO NAZIONALE DI RIPRESA E RESILIENZA (PNRR)—MISSIONE 4 COMPONENTE 2, INVESTIMENTO 1.4—D.D. 1033 17/06/2022, CN00000023). This manuscript reflects only the authors' views and opinions, neither the European Union nor the European Commission can be considered responsible for them.

Conflicts of Interest: The authors declare no conflicts of interest.

Nomenclature

Symbols	
c^{curt}	Curtailment cost [€/kWh]
c_t^{purch}	Electricity purchase price at timestep t [€/kWh]
c_{es}^{TP}	Throughput O&M cost of the energy storage technology
c^{UD}	Unmet demand cost [€/kWh]
dt_1	Timestep duration of the EMS I layer [hours]
l	Lag
$\hat{Load}_{for}$	Load forecast
$Load_{meas}$	Load measurements
$ND_{nd,t}^{curt}$	Average timestep curtailed power [kW] of non-dispatchable generator nd at t
OF	Objective function
$P_{es,\,t}^{disch}$	Average timestep discharge power exchange [kW] of the energy storage technology es at t
$P_t^{grid,purch}$	Average timestep power [kW] purchased from the grid at t
$P_t^{grid,sell}$	Average timestep power [kW] injected to the grid at t
$\hat{PV}_{for}$	PV forecast
PV_{meas}	PV measurements
r_t^{sell}	Electricity selling price at timestep t [€/kWh]
SOE_t^{dev}	SOE deviation [kWh] among energy storage technologies at the end timestep t
t	Timestep
UD_t	Average timestep unmet demand [kW] at t
y_{true}	Vector of true values
$y_{forecast}$	Vector of forecasted values
Greek symbols	
ε_{tot}	Total net electrical forecast
ρ^{dev}	Penalty factor for the SOE deviation between energy storage technologies
Φ_t^{Opex}	Total operational cost at timestep t
Acronyms	
ACN	Adaptive charging network
ANN	Artificial neural network
ARIMA	Autoregressive integrated moving average
B2B	Back-to-back
BESS	Battery energy storage system
CS	Charging station
CSR	Clear-sky radiation
DL	Deep learning
DSM	Demand-side management
ED	Encoder–decoder
EMD	Empirical mode decomposition
EMS	Energy management system
EV	Electric vehicle
EVSE	Electric vehicle supply equipment
GHI	Global horizontal irradiance
HMI	Human–machine interface
HML	Hourly mean lookahead
JPL	Jet Propulsion Laboratory
LSTM	Long short-term memory
MAE	Mean absolute error
MG	Microgrid
MILP	Mixed-integer linear programming
MPC	Model predictive control
PUN	Prezzo Unico Nazionale
PHANN	Physical hybrid artificial neural network
PLC	Programmable logic controller

PV	Photovoltaic
PZ	Prezzo Zonale
RES	Renewable energy sources
REST2	Reference evaluation of solar transmittance, 2 bands
RH	Rolling horizon
RMSE	Root mean squared error
RNN	Recurrent neural network
RO	Robust optimization
SARIMA	Seasonal autoregressive integrated moving average
SMAPE	Symmetric mean absolute percentage error
SOC	State of charge
SOE	State of energy

Appendix A. Energy Management System

Sets	
$\mathcal{ES}$	Set of energy storage units
$\mathcal{ND}$	Set of non-dispatchable generators
$\mathcal{T}_1$	Set of 1st layer timesteps
$\mathcal{T}_2$	Set of 2nd layer timesteps
Continuous variables	
$P^{ch}_{es,\,t}$	Average timestep charge power exchange [kW] of the energy storage technology $es \in \mathcal{ES}$ at time $t \in \mathcal{T}, \in \mathbb{R}^+$
$P^{disch}_{es,\,t}$	Average timestep discharge power exchange [kW] of the energy storage technology $es \in \mathcal{ES}$ at time $t \in \mathcal{T}, \in \mathbb{R}^+$
$P^{net}_{es,\,t}$	Average timestep net power exchange [kW] of the energy storage technology $es \in \mathcal{ES}$ at time $t \in \mathcal{T}, \in \mathbb{R}^+$
$P^{grid,net}_{t}$	Average timestep net grid exchange power [kW] at time $t \in \mathcal{T}, \in \mathbb{R}^+$
$P^{grid,purch}_{t}$	Average timestep power [kW] purchased from the grid at time $t \in \mathcal{T}, \in \mathbb{R}^+$
$P^{grid,sell}_{t}$	Average timestep power [kW] injected to the grid at time $t \in \mathcal{T}, \in \mathbb{R}^+$
$ND^{curt}_{nd,t}$	Average timestep curtailed power [kW] of non − dispatchable generator $nd \in \mathcal{ND}$, at time $t \in \mathcal{T}, \in \mathbb{R}^+$
$ND^{out}_{nd,t}$	Average timestep produced power [kW] of non − dispatchable generator $nd \in \mathcal{ND}$, at time $t \in \mathcal{T}, \in \mathbb{R}^+$
$SOE_{es,\,t}$	State of energy [kWh] of the energy storage technology $es \in \mathcal{ES}$ at the end timestep $t \in \mathcal{T}, \in \mathbb{R}^+$
SOE^{dev}_{t}	SOE deviation [kWh] among energy storage technologies at the end timestep $t \in \mathcal{T}, \in \mathbb{R}^+$
UD_t	Average timestep unmet demand [kW] at time $t \in \mathcal{T}, \in \mathbb{R}^+$
Parameters	
c^{curt}	Curtailment cost [€/kWh]
c^{TP}_{es}	Throughput O&M cos t of the energy storage technology $es \in \mathcal{ES}$ [€/kWh]
c^{purch}_{t}	Electricity purchase price at timestep t [€/kWh]
c^{UD}	Unmet demand cost [€/kWh]
dt_1	Timestep duration of the EMS I layer [hours]
dt_2	Timestep duration of the EMS II layer [hours]
$Load^{fore}_{t}$	24 h-profile of the average timestep residential consumption forecast [kW]
$P^{max,\,ch}_{es}$	Maximum average timestep charge power exchange [kW] of the energy storage technology $es \in \mathcal{ES}$
$P^{max,\,disch}_{es}$	Maximum average timestep discharge power exchange [kW] of the energy storage technology $es \in \mathcal{ES}$
$P^{purch,\,max}$	Maximum average timestep purchase power [kW] from the grid
$P^{sell,\,max}$	Maximum average timestep selling power [kW] from the grid

PV_t^{fore}	24 h-profile of the average timestep PV generation forecast [kW]
r_t^{sell}	Electricity selling price at timestep t [€/kWh]
$size_{es}$	Size [kWh] of the energy storage technology $es \in \mathcal{ES}$
SOE_{es}^{max}	Operational maximum limit for SOE [kWh] of the energy storage technology $es \in \mathcal{ES}$
SOE_{es}^{min}	Operational minimum limit for SOE [kWh] of the energy storage technology $es \in \mathcal{ES}$
η_{es}^{ch}	Charging efficiency of the energy storage technology $es \in \mathcal{ES}$
η_{es}^{disch}	Discharging efficiency of the energy storage technology $es \in \mathcal{ES}$
ρ^{dev}	Penalty factor for the SOE deviation between energy storage technologies

Appendix A.1. First Layer

The first layer of the home EMS is formulated using a deterministic MILP, where all the operational variables and constraints are indexed for every timestep.

The decision variables of the problem are the following:

- Battery average charge $P_{es,\,t}^{ch}$, discharge $P_{es,\,t}^{disch}$, net power exchange $P_{es,\,t}^{net}$, and state of energy $SOE_{es,\,t}$ of storage unit es for each timestep t;
- Average power purchased $P_t^{grid,purch}$ and sold $P_t^{grid,sell}$ into the grid for each timestep t.

Please note that given the discrete nature of the time horizon, the values of those operational variables measured as power (e.g., $P_{es,\,t}^{disch}$ as kW) are considered as timestep average. Therefore, the energy quantities related to the average power at each time interval are obtained by multiplying the variable by the timestep duration dt_1. In the case of hourly timestep duration, then the numerical values related to the average power and energy are exactly the same.

The operational problem aims at defining the strategic planning and economic dispatch of the household by minimizing the total operational costs:

$$OF = min\left(\sum_{t\,\in\,\mathcal{T}_1} \Phi_t^{Opex}\right) \tag{A1}$$

where:

$$\begin{aligned}\Phi_t^{Opex} = c_t^{purch} \quad & \cdot P_t^{grid,purch}\cdot dt_1 - r_t^{sell}\cdot P_t^{grid,sell}\cdot dt_1 \\ & + \sum_{es\in\mathcal{ES}}\left[c_{es}^{TP}\cdot P_{es,\,t}^{disch}\cdot dt_1 + \rho^{dev}\cdot SOE_t^{dev}\right] + c^{curt}\cdot ND_{nd,t}^{curt} \\ & \cdot dt_1 + c^{UD}\cdot UD_t\cdot dt_1\end{aligned} \tag{A2}$$

The total operational costs Φ_t^{Opex} associated to each timestep t are given by the sum of four main components:

- $c_t^{purch}\cdot P_t^{grid,purch}\cdot dt_1 - r_t^{sell}\cdot P_t^{grid,sell}\cdot dt_1$ represents the cost and revenue (negative cost) coming from the withdrawal and injection of power from/into the grid;
- $\sum_{es\in\mathcal{ES}}\left[c_{es}^{TP}\cdot P_{es,\,t}^{disch}\cdot dt_1 + \rho^{dev}\cdot SOE_t^{dev}\right]$ is the sum of the batteries' throughput-based storage O&M cost, and penalty cost associated with their SOE deviations;
- $c^{curt}\cdot ND_{nd,t}^{curt}\cdot dt_1 + c^{UD}\cdot UD_t\cdot dt_1$ are penalty costs for curtailment of RES generation and unmet demands.

The main constraints to which the model is subjected can be summarized as follows:

- Storage dynamic constraints: for each storage unit, the operational behavior describing the charge and discharge power, as well as the evolution in time of the state of charge;
- Grid constraints: the purchase and sold electricity must respect the contract limit of the user;

- Power balance constraints: the overall electricity generated by non-dispatchable units, the energy discharged by the storage, and the energy purchased from the grid must always be equal to the energy charging the storage and the quantity exported to the grid.

Appendix A.2. BESS Operational Constraints

From a modeling point of view, batteries and electric vehicles are approached adopting the same strategy.

Upper bounds on the maximum charge and discharge power, as well as the maximum storage capacity, are defined:

$$P_{es,\,t}^{disch} \leq P_{es}^{max,\,disch} \quad \forall es \in \mathcal{ES}, \forall t \in \mathcal{T}_1 \tag{A3}$$

$$P_{es,\,t}^{ch} \leq P_{es}^{max,\,ch} \quad \forall es \in \mathcal{ES}, \forall t \in \mathcal{T}_1 \tag{A4}$$

Storage systems must respect their maximum and the minimum state of energy:

$$SOE_{es,\,t} \leq SOE_{es}^{max} \quad \forall es \in \mathcal{ES}, \forall t \in \mathcal{T}_1 \tag{A5}$$

$$SOE_{es,\,t} \geq SOE_{es}^{min} \quad \forall es \in \mathcal{ES}, \forall t \in \mathcal{T}_1 \tag{A6}$$

Then, the net power flow from/to the storage is described by the real variable $P_{es,\,t}^{net}$, which considers the charge and discharge efficiencies:

$$P_{es,\,t}^{net} = P_{es,\,t}^{disch} - P_{es,\,t}^{ch} \quad \forall es \in \mathcal{ES}, \forall t \in \mathcal{T}_1 \tag{A7}$$

The SOE evolution in time is then defined by the following constraint, which describes the SOE of the storage at the end of t by taking into account the self-discharge of the unit by means of η_{es}^{SD} and considers the charge and discharge efficiencies:

$$SOE_{es,\,t} = SOE_{es,\,t-1} \cdot \eta_{es}^{SD} + \left(P_{es,\,t}^{ch} \cdot \eta_{es}^{ch} - {}^{P_{es,\,t}^{disch}}/_{\eta_{es}^{disch}} \right) \cdot dt_1 \quad \forall es \in \mathcal{ES}, \forall t \in \mathcal{T}_1 \tag{A8}$$

A correct management of storage systems requires different storage units to follow the same trajectory. This is possible introducing the penalty variable $SOE_{es,t}^{dev}$ and linking it with the absolute value of the difference between the batteries' SOE. The absolute value can be easily linearized:

$$SOE_{t}^{dev} \geq SOE_{BESS\ 1,\,t} - SOE_{BESS\ 2,\,t} \quad \forall t \in \mathcal{T}_1 \tag{A9}$$

$$SOE_{t}^{dev} \geq SOE_{BESS\ 2,\,t} - SOE_{BESS\ 1,\,t} \quad \forall t \in \mathcal{T}_1 \tag{A10}$$

Appendix A.3. Grid Operational Constraints

The power exchanged with the grid is set by the user contract, which introduces a limitation in both the maximum purchase power and the maximum selling power. A binary variable is needed to avoid the withdrawal and injection of power at the same time. In principle, it may be avoided considering a purchase price higher enough than the selling price, but since the price structures may be different, it is conservative to introduce the binary variable to guarantee a feasible decision.

$$P_{t}^{grid,purch} \leq P^{purch,\,max} \cdot z_{t}^{grid} \quad \forall t \in \mathcal{T}_1 \tag{A11}$$

$$P_{t}^{grid,sell} \leq P^{sell,\,max} \cdot \left(1 - z_{t}^{grid}\right) \quad \forall t \in \mathcal{T}_1 \tag{A12}$$

Finally, the net power exchange with the grid is the difference between purchase and sold power:

$$P_{t}^{grid,net} = P_{t}^{grid,purch} - P_{t}^{grid,sell} \quad \forall t \in \mathcal{T}_1 \tag{A13}$$

Appendix A.4. PV Production

The possibility of curtailing part of the non-dispatchable generation has been modeled by the curtailment variable, which is strongly discouraged through a high associated curtailment cost.

$$ND_t^{out} + ND_t^{curt} = ND_t^{fore} \quad \forall t \in \mathcal{T}_1 \tag{A14}$$

Appendix A.5. Electricity Balance

The electricity balance must be guaranteed at each timestep. In particular, the unmet demand term is needed to always assure the constraint feasibility and to understand when the system is not able to cover the house consumption. In fact, the associated unmet demand cost is 100 times the cost of purchasing electricity.

$$ND_t^{out} + P_{es,\,t}^{net} + P_t^{grid,net} + UD_t = Load_t^{fore} \quad \forall t \in \mathcal{T}_1 \tag{A15}$$

Appendix A.6. Second Layer

The second-layer model is a rule-based algorithm that, given the optimal setpoints provided by the first-layer model, decides how to share the net demand forecast error (given by the forecasting error of PV and house consumption) among the components of the system, considering the technical limitations of each unit. The control strategy consists in updating the power setpoints according to the system measurements and so properly interacting with the BESS to balance the microgrid.

The net demand forecast error can be computed as follows:

$$err_t = Load_t^{real} - Load_t^{fore} - \left(ND_t^{real} - ND_t^{fore}\right) \quad \forall t \in \mathcal{T}_2 \tag{A16}$$

Moreover, at each timestep the EV and BESS setpoints' cut reallocation must be addressed. It may be caused by the impossibility of meeting their technical limits:

$$SOE_{es,t}^{plan} = SOE_{es,\,t-1} \cdot \eta_{es}^{SD} + \left(P_{es,\,t}^{ch,setpoint} \cdot \eta_{es}^{ch} - P_{es,\,t}^{disch,setpoint} / \eta_{es}^{disch} \right) \cdot dt_2 \quad \forall t \in \mathcal{T}_2 \tag{A17}$$

$$P_{es,\,t}^{disch,cut} = min\left\{ P_{es,\,t}^{disch,\,setpoint},\ max\left\{ \eta_{es}^{disch} \cdot \frac{SOE_{es}^{min} - SOE_{es,t}^{plan}}{dt_2}, 0 \right\} \right\} \quad \forall t \in \mathcal{T}_2 \tag{A18}$$

$$P_{es,\,t}^{ch,cut} = min\left\{ P_{es,\,t}^{ch,\,setpoint},\ max\left\{ \frac{SOE_{es,t}^{plan} - SOE_{es}^{min}}{\eta_{es}^{ch} \cdot dt_2}, 0 \right\} \right\} \quad \forall t \in \mathcal{T}_2 \tag{A19}$$

$SOE_{es,t}^{plan}$, shown in Equation (A17), is computed at the beginning of the second layer. It reflects the state of energy level that BESS would attain by the end of the timestep if adhering to the power setpoints determined by the strategic decisions made in the first layer. The power setpoint adjustments, Equations (A18) and (A19), are then evaluated by comparing $SOE_{es,t}^{plan}$ with the operational limits of the components and the strategic decisions from the first layer. These power setpoints, combined with the net demand forecast error, collectively define the entire power imbalance that needs to be addressed by the second layer:

$$\Delta P_t = err_t + P_{es,\,t}^{disch,cut} - P_{es,\,t}^{ch,cut} \quad \forall t \in \mathcal{T}_2 \tag{A20}$$

It is possible to distinguish between power deficit and power excess, respectively associated with positive and negative power imbalance. In Figure A1, the second layer block flow scheme shows how the different situations are handled with different priorities. In particular, the rationale behind the selected priorities aims mainly at maintaining the optimal grid setpoint coming from the first layer, and it can be summarized as follows:

1. BESS charge or discharge;
2. Grid withdrawal or injection;
3. Unmet demand or curtailment.

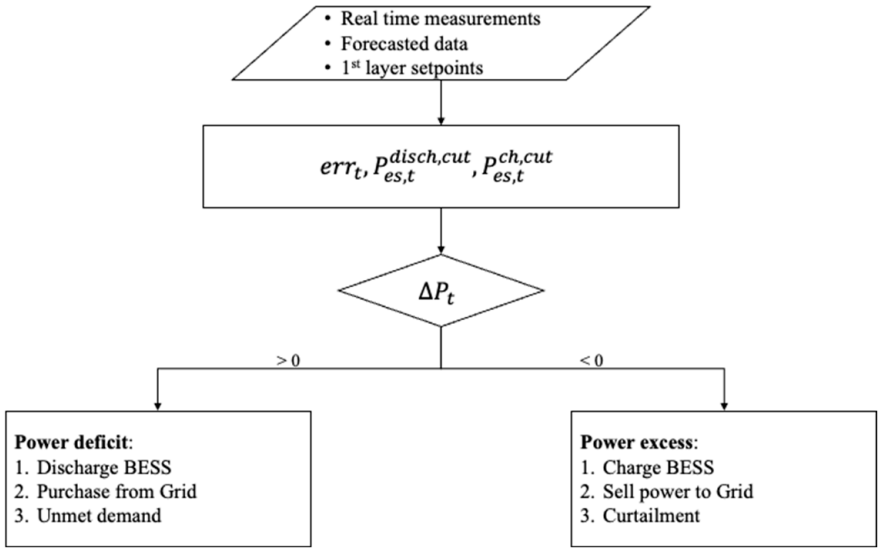

Figure A1. Second layer block scheme.

Appendix B. EV Charging Forecaster

Appendix B.1. Long Short-Term Memory

LSTM is an RNN specifically designed to help the network learn long-term dependencies; it was originally proposed by Hochreiter and Schmidhuber in 1997 [51] and is nowadays widely used in several fields of application, such as natural language and translations [52]. LSTM introduces a new processing unit, the memory cell commonly referred to as 'cell'. To control the memory cell, some gates are needed with internal mechanisms that can regulate the flow of information coming in and out of the cell. The common architecture of the LSTM cell can be observed in Figure A2.

The core concept of the model is the cell state c_t, represented by the horizontal line running through the top of the diagram. It acts as a conveying belt that stores and transfers condensed information all the way down the sequence chain. The content of the cell state changes through time thanks to the interaction of the previously computed output h_{t-1} and the current external input x_t. The circles in Figure A1 are either sigmoid (σ) or tansigmoid (*tanh*) layers. The operations represented in the squares are the point-wise multiplications (X) and point-wise addition (+). In Equation (A20), the governing principles are given. The loss function for training is MSE, which is derived directly from the negative log likelihood of a gaussian probability density function. Two desirable trains are that it is fast to calculation during backpropagation of errors through time and that MSE tends to penalize large errors more than small ones. For training the time series, values are normalized such that the minimum value is zero and maximum is one.

$$\begin{aligned} MSE &= \tfrac{1}{n}\sum(y_{true} - y_{estimated})^2 \\ MAE &= \tfrac{1}{n}\sum(y_{true} - y_{estimated})^2 \end{aligned} \quad \text{(A21)}$$

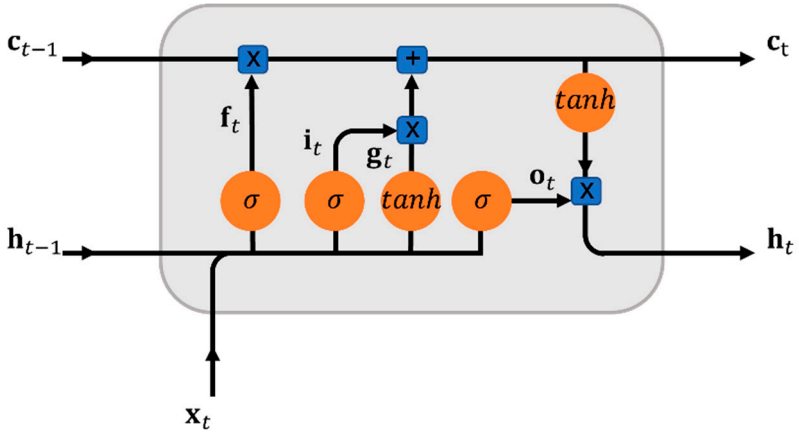

Figure A2. Common architecture of the LSTM cell.

Appendix B.2. Encoder–Decoder/Sequence to Sequence

The load forecast required for a day-ahead unit commitment problem is in the category of many-to-many prediction, since it usually takes as input the time series of power sampled at a certain timestep length and tries to predict another sequence of values; it could require the two sequences to have different lengths. A proper way to handle many-to-many prediction is an encoder–decoder (ED) architecture that consists of three components: an encoder, a context vector, and a decoder. Both the encoder and the decoder are constructed as layers of RNN units. The encoder takes a sequence as the input and transforms it into a context vector, an element with a fixed shape that acts as a condensed representation of the input time series, often called dimensionality reduction. The output of the encoder, the hidden state, is usually the state of the last RNN timestep h_i. The length of the vector is equal to the number of RNN cells in the encoder. The context vector acts as the initial hidden state of the decoder taking the encoder output and feeding it repeatedly to the decoder as input. The decoder is a dimensionality-increasing step that interprets the context vector to make predictions for each timestep required in the output.

Appendix B.3. Attention Mechanism

Attention mechanisms were introduced for the first time in 1997 by Bahdanau in [42]; a similar, modified version was later presented by Luong [53]. They were developed to solve the incapability of ED networks to remember long sequences given as input due to the limited length of the context vector. Important elements for the forecast of the current output could come from any point in the input sequence, but the context vector is not always capable of encapsulating the information "seen" at the beginning of the input sequence. Attention mechanisms try to replicate the human brain's capability of focusing on small portions of the entire information provided at a time, paying attention only to the ones that are relevant to the answer that is required.

In the presence of an attention layer, the encoder functions exactly as in the case of a simple encoder–decoder model producing a hidden state h for each timestep. The context vector is not constant but changes at each timestep; it is calculated as a weighted mean among all the hidden states of the encoder, as shown in Equation (A22).

$$c_t = \alpha_{t,1} h_1 + \alpha_{t,2} h_t + \alpha_{t,m} h_m \quad \text{(A22)}$$

where c_t is the context vector at the current timestep t and h_m is the hidden state of the last timestep in the input with m being the length of the input sequence. The weight $\alpha_{t,i}$ is the alignment weight computed at the i-th timestep. Each α is the result of the application of a softmax function to the attention scores $e_{t,i}$ to normalize them. The attention scores are computed through a proper alignment model $a(.)$, an operation that scores how well the current hidden state of the encoder h_i is matching with the hidden state of the decoder

state s_{t-1} at the previous timestep. Equations (A23) and (A24) illustrate how alignment scores and alignment weights are calculated. The weights favor the hidden states that are matching with the previous output; in this way, the context vector is paying attention only to the parts of the input that are considered relevant by the alignment function solving the problem of the limited length.

$$e_{t,i} = a(h_i, s_{t-1}) \tag{A23}$$

$$\alpha_{,it} = softamx(e_{t,i}) \tag{A24}$$

The decoder takes in as input the context vector, the previous hidden decoder state, and the current output, to compute the final prediction. The attention model described is the one proposed by Bahdanau [42]; in this case, the alignment function is a single-layer perceptron, as shown in Equation (A25):

$$a(s_{t-1}, h_i) = v_a^T \, tanh(W_a s_{i-1} + U_a h_i) \tag{A25}$$

where $W_a \in R^{nxn}$ and $v_a \in R^n$ are weight matrices that are being optimized during the training process to minimize MSE.

Appendix B.4. Persistence

Naive persistence is a benchmark forecast model based on the most trivial assumption that can be made when making predictions. It forecasts the current timestep t using the measurement from the last timestep $t-1$. In this case, the lag value L is 1. In a modified version sometimes called seasonal persistence, the lag value is chosen to match a seasonality in the data, such as daily or weekly in the case of electric load forecasting. As an example, for a time series with strong weekly seasonality, the timestep t is forecasted with the measurement from $t-7d$ or $t-168$ if the time series interval is 1 h. This is described in Equation (A26), where y_f is the forecasted value and y the measured one.

$$y_f(t+1) = y(t-L) \tag{A26}$$

References

1. EEA. EEA Greehouse Gases—Data Viewer. 2023. Available online: https://www.eea.europa.eu/data-and-maps/data/data-viewers/greenhouse-gases-viewer (accessed on 9 April 2024).
2. IEA. Global EV Outlook 2023. Available online: https://www.iea.org/reports/global-ev-outlook-2023 (accessed on 11 April 2024).
3. Alrubaie, A.J.; Salem, M.; Yahya, K.; Mohamed, M.; Kamarol, M. A Comprehensive Review of Electric Vehicle Charging Stations with Solar Photovoltaic System Considering Market, Technical Requirements, Network Implications, and Future Challenges. *Sustainability* **2023**, *15*, 8122. [CrossRef]
4. Wang, L.; Qin, Z.; Slangen, T.; Bauer, P.; Van Wijk, T. Grid Impact of Electric Vehicle Fast Charging Stations: Trends, Standards, Issues and Mitigation Measures—An Overview. *IEEE Open J. Power Electron.* **2021**, *2*, 56–74. [CrossRef]
5. Deeum, S.; Charoenchan, T.; Janjamraj, N.; Romphochai, S.; Baum, S.; Ohgaki, H.; Mithulananthan, N.; Bhumkittipich, K. Optimal Placement of Electric Vehicle Charging Stations in an Active Distribution Grid with Photovoltaic and Battery Energy Storage System Integration. *Energies* **2023**, *16*, 7628. [CrossRef]
6. Rouhani, M.; Ardakanian, O.; Musilek, P. Robust Sizing of Solar-Powered Charging Station with Co-located Energy Storage. In Proceedings of the 2022 IEEE Power & Energy Society General Meeting (PESGM), Denver, CO, USA, 17–21 July 2022; IEEE: Washington, DC, USA, 2022; pp. 1–5. [CrossRef]
7. Yap, K.Y.; Chin, H.H.; Klemeš, J.J. Solar Energy-Powered Battery Electric Vehicle charging stations: Current development and future prospect review. *Renew. Sustain. Energy Rev.* **2022**, *169*, 12862. [CrossRef]
8. Cabrera-Tobar, A.; Blasuttigh, N.; Massi Pavan, A.; Lughi, V.; Petrone, G.; Spagnuolo, G. Energy Scheduling and Performance Evaluation of an E-Vehicle Charging Station. *Electronics* **2022**, *11*, 3948. [CrossRef]
9. Hai, T.; Zhou, J.; Alazzawi, A.k.; Muranaka, T. Management of Renewable-Based Multi-Energy Microgrids with Energy Storage and Integrated Electric Vehicles Considering Uncertainties. *J. Energy Storage* **2023**, *60*, 106582. [CrossRef]
10. Pamulapati, T.; Cavus, M.; Odigwe, I.; Allahham, A.; Walker, S.; Giaouris, D. A Review of Microgrid Energy Management Strategies from the Energy Trilemma Perspective. *Energies* **2022**, *16*, 289. [CrossRef]
11. Wazirali, R.; Yaghoubi, E.; Abujazar, M.S.S.; Ahmad, R.; Vakili, A.H. State-of-the-Art Review on Energy and Load Forecasting in Microgrids Using Artificial Neural Networks, Machine Learning, and Deep Learning Techniques. *Electr. Power Syst. Res.* **2023**, *225*, 109792. [CrossRef]

12. Polimeni, S.; Nespoli, A.; Leva, S.; Valenti, G.; Manzolini, G. Implementation of Different PV Forecast Approaches in a MultiGood MicroGrid: Modeling and Experimental Results. *Processes* **2021**, *9*, 323. [CrossRef]
13. Cabrera-Tobar, A.; Massi Pavan, A.; Petrone, G.; Spagnuolo, G. A Review of the Optimization and Control Techniques in the Presence of Uncertainties for the Energy Management of Microgrids. *Energies* **2022**, *15*, 9114. [CrossRef]
14. Said, D. Intelligent Photovoltaic Power Forecasting Methods for a Sustainable Electricity Market of Smart Micro-Grid. *IEEE Commun. Mag.* **2021**, *59*, 122–128. [CrossRef]
15. Said, D. A Decentralized Electricity Trading Framework (DETF) for Connected EVs: A Blockchain and Machine Learning for Profit Margin Optimization. *IEEE Trans. Ind. Inf.* **2021**, *17*, 6594–6602. [CrossRef]
16. Singh, B.; Dubey, P.K.; Kumar, V.; Singh, D. A Novel Approach for Comparative Analysis of Distributed Generations and Electric Vehicles in Distribution Systems. *Electr. Eng.* **2024**, *106*, 2371–2390. [CrossRef]
17. Zhu, J.; Yang, Z.; Chang, Y.; Guo, Y.; Zhu, K.; Zhang, J. A Novel LSTM Based Deep Learning Approach for Multi-Time Scale Electric Vehicles Charging Load Prediction. In Proceedings of the 2019 IEEE Innovative Smart Grid Technologies—Asia (ISGT Asia), Chengdu, China, 21–24 May 2019; IEEE: Washington, DC, USA, 2019; pp. 3531–3536.
18. Hippert, H.S.; Pedreira, C.E.; Souza, R.C. Neural Networks for Short-Term Load Forecasting: A Review and Evaluation. *IEEE Trans. Power Syst.* **2001**, *16*, 44–55. [CrossRef]
19. Calearo, L.; Marinelli, M.; Ziras, C. A Review of Data Sources for Electric Vehicle Integration Studies. *Renew. Sustain. Energy Rev.* **2021**, *151*, 111518. [CrossRef]
20. Gao, Q.; Lin, Z.; Zhu, T.; Zhou, W.; Wang, G.; Zhang, T.; Zhang, Z.; Waseem, M.; Liu, S.; Han, C. Charging Load Forecasting of Electric Vehicle Based on Monte Carlo and Deep Learning. In Proceedings of the 2019 IEEE Sustainable Power and Energy Conference (iSPEC), Beijing, China, 21–23 November 2019; IEEE: Washington, DC, USA, 2019; pp. 1309–1314.
21. Al-Ogaili, A.S.; Tengku Hashim, T.J.; Rahmat, N.A.; Ramasamy, A.K.; Marsadek, M.B.; Faisal, M.; Hannan, M.A. Review on Scheduling, Clustering, and Forecasting Strategies for Controlling Electric Vehicle Charging: Challenges and Recommendations. *IEEE Access* **2019**, *7*, 128353–128371. [CrossRef]
22. Bianchi, F.M.; Maiorino, E.; Kampffmeyer, M.C.; Rizzi, A.; Jenssen, R. *An Overview and Comparative Analysis of Recurrent Neural Networks for Short Term Load Forecasting*; Springer: Berlin/Heidelberg, Germany, 2017. [CrossRef]
23. Wood, M.; Ogliari, E.; Nespoli, A.; Simpkins, T.; Leva, S. Day Ahead Electric Load Forecast: A Comprehensive LSTM-EMD Methodology and Several Diverse Case Studies. *Forecasting* **2023**, *5*, 297–314. [CrossRef]
24. Kouka, K.; Masmoudi, A.; Abdelkafi, A.; Krichen, L. Dynamic Energy Management of an Electric Vehicle Charging Station Using Photovoltaic Power. *Sustain. Energy Grids Netw.* **2020**, *24*, 100402. [CrossRef]
25. Bui, V.-H.; Hussain, A.; Zarrabian, S.; Kump, P.M.; Su, W. Clustering-Based Optimal Operation of Charging Stations under High Penetration of Electric Vehicles. *Sustain. Energy Grids Netw.* **2023**, *36*, 101178. [CrossRef]
26. Engelhardt, J.; Zepter, J.M.; Gabderakhmanova, T.; Marinelli, M. Energy Management of a Multi-Battery System for Renewable-Based High Power EV Charging. *eTransportation* **2022**, *14*, 100198. [CrossRef]
27. Jiang, W.; Zhen, Y. A Real-Time EV Charging Scheduling for Parking Lots With PV System and Energy Store System. *IEEE Access* **2019**, *7*, 86184–86193. [CrossRef]
28. Wang, Z.; Jochem, P.; Fichtner, W. A Scenario-Based Stochastic Optimization Model for Charging Scheduling of Electric Vehicles under Uncertainties of Vehicle Availability and Charging Demand. *J. Clean. Prod.* **2020**, *254*, 119886. [CrossRef]
29. Wu, J.; Liu, Y.; Chen, X.; Wang, C.; Li, W. Data-Driven Adjustable Robust Day-Ahead Economic Dispatch Strategy Considering Uncertainties of Wind Power Generation and Electric Vehicles. *Int. J. Electr. Power Energy Syst.* **2022**, *138*, 107898. [CrossRef]
30. Zehra, S.S.; Wood, M.J.; Grimaccia, F.; Leva, S.; Mussetta, M. Solar and Grid Power Integration for Dynamic Energy Management in Electric Vehicle Charging and Load Fulfilment with Fuzzy Logic. In Proceedings of the 2023 AEIT International Conference on Electrical and Electronic Technologies for Automotive (AEIT AUTOMOTIVE), Modena, Italy, 17–19 July 2023; IEEE: Washington, DC, USA, 2023; pp. 1–6.
31. Garcia-Trivino, P.; Torreglosa, J.P.; Fernandez-Ramirez, L.M.; Jurado, F. Decentralized Fuzzy Logic Control of Microgrid for Electric Vehicle Charging Station. *IEEE J. Emerg. Sel. Top. Power Electron.* **2018**, *6*, 726–737. [CrossRef]
32. Dukpa, A.; Butrylo, B. MILP-Based Profit Maximization of Electric Vehicle Charging Station Based on Solar and EV Arrival Forecasts. *Energies* **2022**, *15*, 5760. [CrossRef]
33. Moretti, L.; Polimeni, S.; Meraldi, L.; Raboni, P.; Leva, S.; Manzolini, G. Assessing the Impact of a Two-Layer Predictive Dispatch Algorithm on Design and Operation of off-Grid Hybrid Microgrids. *Renew. Energy* **2019**, *143*, 1439–1453. [CrossRef]
34. Pascual, J.; Barricarte, J.; Sanchis, P.; Marroyo, L. Energy Management Strategy for a Renewable-Based Residential Microgrid with Generation and Demand Forecasting. *Appl. Energy* **2015**, *158*, 12–25. [CrossRef]
35. Luna, A.C.; Diaz, N.L.; Graells, M.; Vasquez, J.C.; Guerrero, J.M. Mixed-Integer-Linear-Programming-Based Energy Management System for Hybrid PV-Wind-Battery Microgrids: Modeling, Design, and Experimental Verification. *IEEE Trans. Power Electron.* **2017**, *32*, 2769–2783. [CrossRef]
36. Parisio, A.; Rikos, E.; Glielmo, L. Stochastic Model Predictive Control for Economic/Environmental Operation Management of Microgrids: An Experimental Case Study. *J. Process Control* **2016**, *43*, 24–37. [CrossRef]
37. Parisio, A.; Rikos, E.; Tzamalis, G.; Glielmo, L. Use of Model Predictive Control for Experimental Microgrid Optimization. *Appl. Energy* **2014**, *115*, 37–46. [CrossRef]

38. Marzband, M.; Sumper, A.; Ruiz-Álvarez, A.; Domínguez-García, J.L.; Tomoiagă, B. Experimental Evaluation of a Real Time Energy Management System for Stand-Alone Microgrids in Day-Ahead Markets. *Appl. Energy* **2013**, *106*, 365–376. [CrossRef]
39. MG2Lab. Available online: https://www.mg2lab.polimi.it/ (accessed on 17 April 2024).
40. Lee, E.-K.; Shi, W.; Gadh, R.; Kim, W. Design and Implementation of a Microgrid Energy Management System. *Sustainability* **2016**, *8*, 1143. [CrossRef]
41. Polimeni, S.; Moretti, L.; Manzolini, G.; Leva, S.; Meraldi, L.; Raboni, P. Numerical and Experimental Testing of Predictive EMS Algorithms for PV-BESS Residential Microgrid. In Proceedings of the 2019 IEEE Milan PowerTech, Milano, Italy, 23–27 June 2019; IEEE: Washington, DC, USA, 2019; pp. 1–6.
42. Bahdanau, D.; Cho, K.; Bengio, Y. Neural machine translation by jointly learning to align and translate. *arXiv* **2016**, arXiv:1409.0473v7.
43. Nespoli, A.; Mussetta, M.; Ogliari, E.; Leva, S.; Fernández-Ramírez, L.; García-Triviño, P. Robust 24 Hours Ahead Forecast in a Microgrid: A Real Case Study. *Electronics* **2019**, *8*, 1434. [CrossRef]
44. Molteni, F.; Buizza, R.; Palmer, T.N.; Petroliagis, T. The ECMWF Ensemble Prediction System: Methodology and Validation. *Q. J. R. Meteorol. Soc.* **1996**, *122*, 73–119. [CrossRef]
45. Stein, J.; Hansen, C.; Reno, M. *Global Horizontal Irradiance Clear Sky Models: Implementation and Analysis*; No. SAND2012-2389; Sandia National Laboratories (SNL): Albuquerque, NM, USA; Livermore, CA, USA, 2012.
46. Abadi, M.; Agarwal, A.; Barham, P.; Brevdo, E.; Chen, Z.; Citro, C.; Corrado, G.S.; Davis, A.; Dean, J.; Devin, M.; et al. TensorFlow: Large-Scale Machine Learning on Heterogeneous Distributed Systems. 2016. Available online: https://www.tensorflow.org/ (accessed on 18 April 2024).
47. Dolara, A.; Grimaccia, F.; Leva, S.; Mussetta, M.; Ogliari, E. A Physical Hybrid Artificial Neural Network for Short Term Forecasting of PV Plant Power Output. *Energies* **2015**, *8*, 1138–1153. [CrossRef]
48. Bynum, M.L.; Hackebeil, G.A.; Hart, W.E.; Laird, C.D.; Nicholson, B.L.; Siirola, J.D.; Watson, J.-P.; Woodruff, D.L. *Woodruff, Pyomo–Optimization Modeling in Python*, 3rd ed.; Springer International Publishing: Cham, Switzerland, 2021; Volume 67, ISBN 978-3-030-68927-8.
49. Lee, Z.J.; Li, T.; Low, S.H. ACN-Data. In Proceedings of the Tenth ACM International Conference on Future Energy Systems, Phoenix, AZ, USA, 25–28 June 2019; ACM: New York, NY, USA, 2019; pp. 139–149.
50. Gestore Dei Mercati Energetici. Available online: https://www.mercatoelettrico.org/ (accessed on 22 April 2024).
51. Hochreiter, S.; Schmidhuber, J. Long Short-Term Memory. *Neural. Comput.* **1997**, *9*, 1735–1780. [CrossRef]
52. Wang, S.; Jiang, J. Learning Natural Language Inference with LSTM. In Proceedings of the 2016 Conference of the North American Chapter of the Association for Computational Linguistics: Human Language Technologies, San Diego, CA, USA, 12–17 June 2016; Association for Computational Linguistics: Stroudsburg, PA, USA, 2016; pp. 1442–1451.
53. Luong, M.-T.; Pham, H.; Manning, C.D. Effective Approaches to Attention-Based Neural Machine Translation. *arXiv* **2015**. [CrossRef]